IET Research Journals

Research Article

IET Journals
The Institution of Engineering and Technology

ISSN 1751-8644
doi: 0000000000
www.ietdl.org

Sizing HESS as Inertial and Primary Frequency Reserve in Low Inertia Power System

Umer Akram[1], *N. Mithulananthan*[1*], *Rakibuzzaman Shah*[2], *S. Ali Pourmousavi*[3]

[1] *School of Information Technology and Electrical Engineering, University of Queensland, Brisbane, Australia*
[2] *School of Science Engineering and Information Technology, Federation University, Mt Helen, VIC-3353, Ballarat, Australia*
[3] *School of Electrical and Electronic Engineering, The University of Adelaide, SA 5005, Adelaide, Australia*
* *E-mail: mithulan@itee.uq.edu.au*

Abstract: Energy storage systems are recognized as the potential solution to alleviate the impacts of reduced inertia and intermittency in power systems due to the integration of renewable energy sources. Several energy storage technologies are available in the market with diverse power and energy characteristics, operational limitations, and costs. Besides, frequency regulations in power systems have different requirements, e.g., inertial response requires high power for short period while primary frequency regulation requires steady power for a longer time. Thus, it is crucial to find out the optimum sizes and types of storage technologies for these services. In this paper, a methodology for sizing fast responsive energy storage technologies for inertial response, primary frequency regulation, and both inertial response and primary frequency regulation is developed. The sizing of storage systems for inertial response, primary frequency regulation, and both inertial response and primary frequency regulation is done separately. The sizing of storage for inertial response is done in two steps. A region reduction iterative algorithm is proposed to estimate the storage size for inertial response. The sizing of the storage system for primary frequency regulation is done analytically. The sizing methodology incorporates the frequency dynamics of storage, converters, and other associated controls that affect the frequency response. Moreover, an economic analysis is carried out to find the optimum combination of storage technologies for inertial response, primary frequency regulation, and both inertial response and primary frequency regulation services. The accuracy of the proposed sizing method has been compared with the metaheuristic algorithm based technique. The effectiveness of the proposed method is also compared with those in the literature. Simulation results show that the proposed method outperforms the existing methods in the literature. Finally, the non-linear simulations revealed the validity of the optimal solutions.

1 Introduction

Large scale integration of renewable energy sources (RES) in power systems reduces inertia [1]. The electric power grids are facing challenges inflicted by low inertia. In Australia, the aggregated capacity of solar photovoltaic (PV) and wind generation (WG) is more than 20% (of the total installed capacity) with a rapid per annum increment. Moreover, the extension of multiple units in existing RES has been proposed with concerns regarding inertia distribution [2]. In the Nordic grid, nuclear power plants are already replaced by RES, and the system operator stated 'low inertia' as one of the three main future challenges for the system [3]. Similarly, in EirGrid and SONI, the current installed capacity of WG is about 3,320 MW with an additional 730 MW to be commissioned by 2020. Despite the great potential, sporadic nature of wind limits the capacity credit of wind [4]. In Central Europe, the system operators investigated the impact of decreasing system inertia on frequency behaviour. It has been reported that the system frequency remains within acceptable limits with reduced inertia in the interconnected system. However, for the split operation after disturbance, the low inertia may result in an instability [5]. In the ERCOT, 20% of the total generation capacity from WG covers around 54% of the instantaneous power. Given the plans for further expansion of WG capacity, ERCOT has already evaluated the market-based solutions to ensure the availability of inertia in the system [6].

Battery energy storage (BES) is anticipated as a potential solution to alleviate the impacts of inertia reduction and intermittency associated with the integration of RES. The ideal characteristics of the energy storage system (ESS) for providing grid ancillary services (especially frequency regulation) are high power density, high energy density, lower cost, and larger cycle life [7]. The power density of the battery is much smaller as compared to energy density. In the BES, the power density needs to be sufficiently high to supply the peak demand. Although the high-power density batteries are available in the market, but, their cost is higher as compared to their lower power density counterparts. This problem can be solved by increasing the BES size which would be costly for utilities. Moreover, the high C-rate operation of BES may raise the safety issues due to thermal runaway [8]. Thus, it is beneficial to combine a high-power dense ESS with BES, which can be used as a buffer to handle the high surge currents economically and efficiently [9].

The hybrid energy storage system (HESS) could be a potential solution to the prior stated issues. The BES can be combined with the high-power dense technologies such as supercapacitor energy storage (SCES), superconducting magnetic energy storage (SMES), and flywheel energy storage (FES) [7]. Unlike BES, the SCES, SMES, FES have high power density, lower energy density, the lower capital cost associated with power density, longer lifetime, and higher capital cost associated with the energy density. The normalized power and energy characteristics of BES, SCES, SMES, and FES are given in Fig. 1. It can be observed from Fig. 1 that the SCES, SMES, and FES have complimentary characteristics compared to BES. Hence, the HESS obtained by combining BES with SCES, SMES, and FES may have the characteristics of an ideal ESS (i.e., high power and energy density, longer cycle life, lower cost associated to energy and power density).

In addition to the type of storage it also is essential to determine the accurate size of the ESS. The under-sized storage may jeopardize the reliable operation of the system, while over-sized storage may require high network investment. Different methodologies have been proposed in the literature to size ESS. In [10] sizing of HESS (BES-SCES) is done to limit the deviations in frequency. The sizing problem is formulated as a cost minimization problem and solved using metaheuristic optimisation algorithm. In addition, a fuzzy

logic based control is also developed to operate the HESS. The control is based on the fact that the fast frequency deviations are supplied by SCES and moderate deviations in the frequency are supplied by BES. In [11], sizing of ESS is done to provide FR. The sizing problem is formulated as cost minimization problem and solved using the particle swarm optimization algorithm. In [12], sizing of energy storage is done for IR and PFR. The sizing methodology is based upon the equivalent inertia estimation which can result in over-sizing. Furthermore, derivative control is used to supply the IR which can result in incorrect operation of storage. The output of ESS for PFR is controlled using the droop control. In [13], bat optimization algorithm is used to size the storage providing primary frequency support. In [14], fuzzy proportional plus differential controller is used to provide the frequency regulation from ESS. The control of ESS is also developed to provide improved frequency regulation [15, 16]. In [17], the capacity estimation of HESS, providing frequency regulation, is formulated as a cost minimization problem. The cost optimization problem is solved using a metaheuristic optimization technique to minimize the initial investment, operation and maintenance costs of storage. The proposed sizing strategy takes into account the complementary characteristics of SCES and BES in order to maximize the profit. In [18], BES-SCES hybrid storage is deployed to provide IR and PFR. The output of SCES is controlled by derivative control and the power output of BES is regulated using droop control.

In addition to ESS, the potential of RES and demand side management to provide frequency regulation have been discussed in [7]. Deloading mode and the inertia emulation are the two main reported techniques for RES to provide frequency regulation [19]. The response from renewable energy sources to provide frequency regulation depends on the availability of the wind speed for wind turbine and time of day and weather for solar PV. There is a chance that the renewable energy sources produce no power at the time of the frequency events. Thus, they are not reliable resources as the response depends on the uncontrollable natural resources. In addition, the frequency events are not very frequent, thus, operating the RES in deloading mode may not be economically appealing. Similarly, the frequency response from demand side management involves sophisticated communication and control mechanisms [7]. The unpredictable customer behaviours could be challenging for the seamless implementation of such methods. Hence, among all the available technologies, ESS is the most reliable and flexible solution, though expensive, to provide frequency ancillary services. To that end, optimal accurate size estimation of ESS is necessary to achieve economical operation.

Most of the research related to the application of ESS for frequency regulation are focused on the capacity estimation of ESS to provide dynamic frequency regulation. In these studies, the sizing problem is formulated as a standard cost minimization problem. Very few studies have done the planning of ESS for dedicated IR and PFR services. In most of these studies the capacity of energy storage is estimated while considering the constraints inflicted by the controllers. In real power systems, however, the output of the reserves dedicated for fast frequency response (IR and PFR) is not controlled by any other controller (PID control, robust control, etc). In fact, the inertial reserve (fast frequency response reserve) is deployed when a contingency appears and its output follows predetermined dispatchment/detachment criteria provided by the system operator [20]. In addition, most of the studies have considered single storage technology, whereas in this paper a technology selection approach is proposed to determine the best combination of technologies for IR-PFR. In this paper, a methodology is developed for planning of single ESS to provide IR, PFR, and HESS for IR-PFR. The proposed planning methodology estimates the required power and energy capacities and determines the most suitable types of storage technologies for IR, PFR, and IR-PFR. A region reduction iterative algorithm (RRIA) is developed to size ESS for IR. The sizing of ESS for PFR is done analytically. The proposed methodology is derived from power system frequency characteristics. The proposed technique is easy to implement and require lower computational effort since it does not utilize metaheuristic algorithm. The accuracy of the proposed methodology is assessed by comparing it with

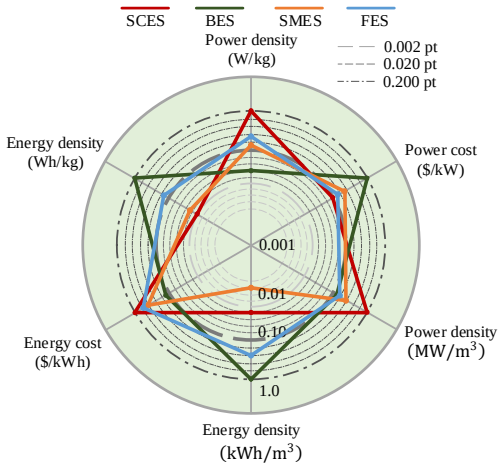

Fig. 1: Normalized power and energy characteristics of ESS.

the teacher learner based optimization (TLBO) algorithm and the technique given in [12].

The remainder of the paper is organized as follows. The overview of the power system frequency characteristics and modelling is briefly described in Section 2. The proposed methodology is illustrated in Section 3, followed by results and discussions in Section 4. Section 5 concludes the paper.

2 Overview and Modelling

2.1 Power System Characteristics

The typical variation in frequency after the occurrence of an outage and the necessary control actions taken to ameliorate its impact is depicted in Fig. 2. The first stage is the natural response from synchronous machines (known as IR) in which the synchronous machines oppose the reduction in frequency by releasing the kinetic energy stored in rotating masses. This stage is followed by the primary frequency control which stabilizes the frequency to the new steady-state value. Then, the load frequency control stage (usually deploys proportional-integral (PI) controller) to recover the frequency to its nominal value. The time of deployment and magnitude of the first two stages is critical as they influence the frequency nadir and RoCoF [21]. The frequency nadir and RoCoF also depend upon the inertia of power system, which can be calculated as (1).

$$H = \frac{E_{kinetic}}{S_{rated}} = \frac{1}{2}\frac{J\omega^2}{S_{rated}} \tag{1}$$

In (1), H is the inertia constant, $E_{kinetic}$ is the kinetic energy stored in the rotor of the synchronous machine rotating at the speed of ω, J is the moment of inertia, and S_{rated} is the power rating. The modern power systems employ large share of RES. The RES can also provide IR if appropriate control is deployed. For example, WG can provide 0.1 pu extra power for 10 sec if the wind speed is more than 6.5 m/s. The WG and PV system can also provide frequency regulation services when operated in de-loaded mode. The power output of RES depend on the intermittent natural resources, i.e., wind speed and solar irradiation. Thus, it is possible that at the time of contingency the power output of RES is zero. In addition, operating the PV or WG in de-loaded mode results in loss of power (which is not economical) as the high RoCoF events do not occur very often. Therefore, in this, work it is assumed that IR is only provided by the conventional generation system. Normally, there are several synchronous machines in a power system. Therefore, the combined inertia constant of the system can be calculated using (2) [22].

$$H_{sys} = \frac{\sum_{i=1}^{n} H_i S_i}{S_{sys}} \tag{2}$$

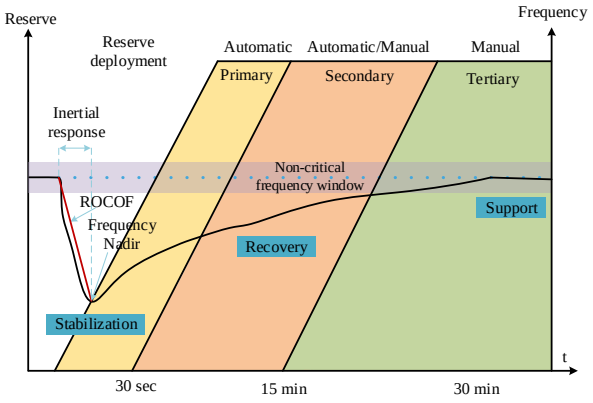

Fig. 2: Frequency response stages defined by the ENTSO-E.

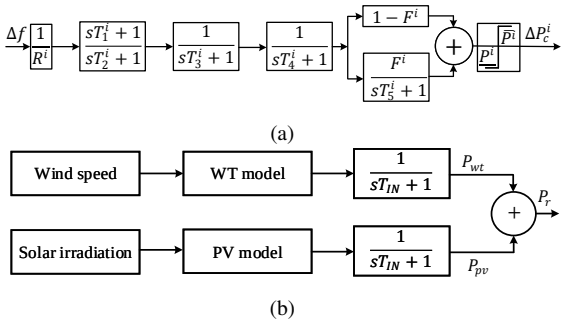

Fig. 3: (a) Block diagram of governor and turbine model (b) Block diagram of RES system.

In (2), H_i is the inertia constant of i^{th} machine with rated power S_i, and S_{sys} is the rating of the overall system. The variation of frequency in small power system is global phenomenon, which can be approximated by using (3) [23].

$$\frac{2H_{sys}}{f}\frac{df}{dt} = \frac{P_g - P_l}{S_{sys}} = \frac{\Delta P}{S_{sys}} \tag{3}$$

In (3), $\frac{df}{dt}$ is the RoCoF, P_g is the total power generated, P_l is the power demand, ΔP is the power deficit, and f is the nominal frequency. The RoCoF is inversely related to inertia constant H. Therefore, the system with higher value of H would experience the lower RoCoF with compared to system with smaller inertia.

2.2 Modelling of Generation System

A generic 12 bus-system is used in this study. The complete data of the system can be found in [24]. The system has four generation plants that employ fossil steam units and hydro units. The block diagram of governor and turbine is shown in Fig. 3a. In the figure, Δf is the deviation in frequency, T_{1-5} are the time constants, ΔP_c is the power output, and $\underline{P}$, $\overline{P}$ are minimum and maximum power capacities. The superscript i depicts parameters of the i^{th} generator. The total power generated by the conventional power plants is $\Delta P_c = \sum_{i=1}^{n} \Delta P_c^i$, where, P_c is the power generated by conventional generators, n is the total number of such generators in the system.

Some of the conventional generators in the system are replaced by the RES e.g. WG and PV. The details in this regard are given in Section 4. The power output of WG can be estimated by (4) [15].

$$P_w = \frac{1}{2} v_r^3 A_{wt} \sigma C_p(\gamma, \rho) \tag{4}$$

In (4), P_w is power output of wind generation system, v_r is the rated wind speed, A_{wt} is the rotor swept area, σ represents air density, and C_p is the power coefficient of the rotor blades. The C_p can be approximated using (5) [15].

$$C_p(\gamma, \rho) = C_1 \times \left(\frac{C_2}{\gamma_i} - C_3\rho - C_4\rho^2 - C_5\right) \times e^{-C_6/\gamma_i} + C_7\gamma_i \tag{5}$$

In (5), ρ is the pitch angle, γ_i, is intermittent tip speed ratio, and γ_i is the optimal tip speed ratio which can be determined as $\gamma_i = \frac{\omega_t \times r_t}{v_r}$, where r_t is radius of rotor. The intermittent tip speed ratio is calculated as in (6) [15].

$$\gamma_i = \frac{(\rho^3 + 1) \times (\gamma_i + 0.08\rho)}{(\rho^3 + 1) - 0.035\,(\gamma_i + 0.08\rho)} \tag{6}$$

Furthermore, the PV system harvests energy from solar irradiation. The power output of a PV system mainly depends on the solar irradiation, efficiency of solar panel, size of solar panel, and the atmospheric temperature. The power output of the solar PV system can be determined as in (7).

$$P_{pv} = \eta_{pv} A_{pv} I (1 - 0.0005(T_o - 25)) \tag{7}$$

In (7), P_{pv} is the power output of PV generation system, η_{pv} is efficiency, A_{pv} area of PV panel, I is the solar irradiation, and T_o is the atmospheric temperature.

Since both PV and WG are connected to the host AC system via inverters, therefore, they cannot provide FR services inherently. However, with adequately deployed auxiliary control in PV and WG, they can participate in the FR services. Both PV and WG are non-dispatchable and harvest power from stochastic natural resources. Hence, it might be possible that at the time of the major event, the power output of PV and WG is zero. Therefore, it is assumed that both PV and WG are connected to the system via inverter without any auxiliary control for FR services (shown in Fig. 3b). The inverter is represented by a first-order lag model with the time constant T_{IN}. This particular model of the inverter is suitable for frequency response studies, and further details of this model can be found in [22]. The total power generated by RES is the sum of the PV and WG output power, $P_r = P_{PV} + P_{WG}$, where, P_r is the total power generated by RES. Therefore, the total power generated in the system is the sum of the output power of RES and conventional generators, $P_g = P_c + P_r$.

2.3 Energy Storage System Model

Typically, the IR and PFR stages are separated in time frame as given in Fig. 2. Hence, the energy storage systems deployed for IR and PFR can be controlled independently. Therefore, the subscripts 'ir' and 'pfr' are used in this study to denote the storage deployed for IR and PFR, respectively. The variation in energy level of ESS is determined by (8).

Charge:

$$E_{ir/pfr}(t + \Delta t) = E_{ir/pfr}(t) + \Delta t P_{ir/pfr}(t) \eta^c_{ir/pfr} \quad \forall t > 0 \tag{8}$$

Disharge:

$$E_{ir/pfr}(t + \Delta t) = E_{ir/pfr}(t) - \Delta t \frac{P_{ir/pfr}(t)}{\eta^d_{ir/pfr}} \quad \forall t > 0 \tag{9}$$

Subjected to power and energy (SoC) bounds

$$\underline{\Omega_{ir/pfr}} \le E_{ir/pfr}(t) \le \overline{\Omega_{ir/pfr}} \quad \forall t > 0 \tag{10}$$

$$-\overline{P_{ir/pfr}} \le P_{ir/pfr}(t) \le \overline{P_{ir/pfr}} \quad \forall t > 0 \tag{11}$$

In (8)-(11), $E_{ir/pfr}$ is the stored energy, $\eta^c_{ir/pfr}$ and $\eta^d_{ir/pfr}$ are charging and discharging efficiency, $\overline{\Omega_{ir/pfr}}$ and $\underline{\Omega_{ir/pfr}}$ are maximum

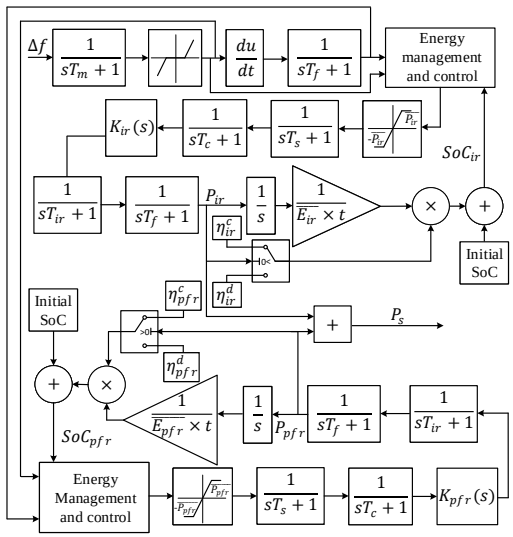

Fig. 4: Frequency response model of HESS.

and minimum energy capacity limits, and $\overline{P_{ir/pfr}}$ is the rated power capacity of ESS. Equation (9) represents the charging of ESS while (10) represents the discharging of ESS.

The total power injected by ESS to power system can be calculated by using (12).

$$P_s(t) = P_{ir}(t) + P_{pfr}(t) \quad \forall t > 0 \tag{12}$$

In (12), P_s is the power output of ESS, P_{ir} is the power output of storage deployed to provide IR, P_{pfr} is the output of storage dedicated for PFR.

In this study, a HESS is deployed for IR and PFR services. HESS consists of two storage technologies, typically a high power dense technology (SCES) and a high energy dense technology (BES). In this study HESS refers to BES-SCES. A frequency response model of HESS is developed for frequency (IR and PFR) studies shown in Fig. 4. In the figure, Δf is deviation in frequency, SoC_{ir} is the state of charge of storage deployed for IR services, SoC_{pfr} is the state of charge of storage deployed for PFR, K_{ir} and K_{pfr} are tthe gains of inertial and PFR control loops, respectively, T_c, T_m, and T_f are the time constants of converter, measuring device, and filter, and T_{ir} and T_{pfr} are the time constants that account for the time required by the storage systems to activate fully once started conduction. The RoCoF is used for the activation of IR reserve, once the storage receives the activation signal, the reserve is deployed into the system. Since the primary purpose of this study is to find the appropriate size and type of storage for the secure operation of small power system with high penetration of RES. The challenges related to the accurate measurement of RoCoF are out of the scope of this study. Therefore, it is assumed that the measurement devices are accurately detecting the RoCoF.

3 Proposed Methodology

In the subsequent subsections, the methodologies will be developed to estimate the size and type of ESS for IR, PFR, and IR-PFR services.

3.1 Sizing ESS for IR

The swing equation of power system with conventional generators, RES, and ESS can be approximated using (13).

$$\frac{2H_{sys}}{f}\frac{df}{dt} = \frac{P_c + P_r - P_l - P_{ir}(\mathbf{1}_{(P_c+P_r>P_l)} - \mathbf{1}_{(P_c+P_r<P_l)})}{S_{sys}} \tag{13}$$

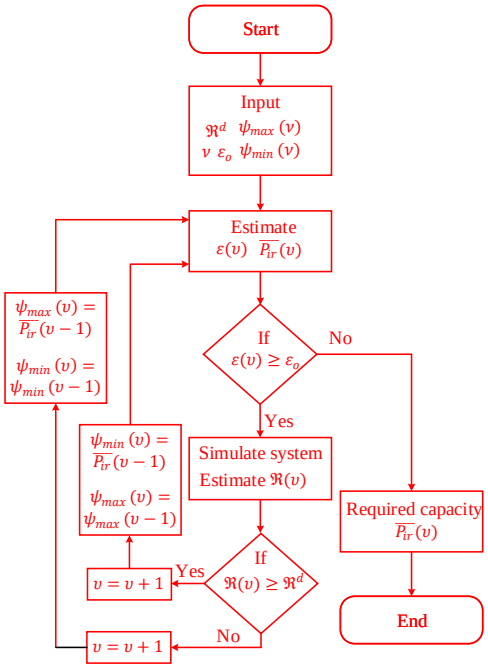

Fig. 5: Flowchart of region reduction iterative algorithm (RRIA).

In (13), $\mathbf{1}_{(\star)}$ is indicator function, which can take a value of 0 or 1. It can be observed from (13) that P_{ir} tries to balance the generation-demand imbalance. Based on the frequency responses of 10 MW BES at Kilroot Power Station (in Northern Ireland [21]) to a disturbance that caused the frequency reduction, P_{ir} can be approximated as in (14).

$$P_{ir} = (1 - e^{-at})(\overline{P_{ir}}\mathbf{1}_{(|\Delta P| \geq \overline{P_{ir}})} + (\mid \Delta P \mid)\mathbf{1}_{(|\Delta P| < \overline{P_{ir}})}) \tag{14}$$

In (14), a is the response time which depends on T_m, T_c, T_f, and T_{ir}. Furthermore, $\Delta P = P_c + P_r - P_l$. To study the impact of storage on frequency response of system, ΔP can be assumed constant over a small period of time. Also, without loss of generality it can be assumed that $P_c + P_r < P_l$ and $\mid \Delta P \mid > \overline{P_{ir}}$. Using these assumptions in (14) and substituting back in (13) gives;

$$\frac{df}{dt} = K\Delta P - K\overline{P_{ir}}(1 - e^{-at}) \tag{15}$$

In (15), $K = \frac{f}{2H_{sys} \times S_{sys}}$. From (15), it is clear that the RoCoF can be limited by the power capability and response time of storage (i.e., an ESS with high power supply capability and lower ramp rate would result in lower RoCoF). The frequency nadir point highly depends on the magnitude of reserve deployed before it is reached. Hence, a storage system with faster ramp up time and high-power rating can result in lower RoCoF and frequency nadir.

The power system planning requires that it must be able to withstand a contingency such as the loss of the largest generator. In such contingency situation, equation (15) can be approximated by (16).

$$\frac{df}{dt} = K'\Delta P - K'\overline{P_{ir}}(1 - e^{-at}) \tag{16}$$

In (16), $K' = \frac{f}{2H'_{sys} \times S'_{sys}}$, H'_{sys} and S'_{sys} are the modified equivalent inertia of system and MVA rating, respectively. The required MW size of ESS to limit RoCoF to any desired value can be computed

IET Research Journals, pp. 1–10

using (17).

$$\overline{P_{ir}} = \lfloor \Delta P - \Re^d \times \frac{1}{K'} \rceil \times \frac{1}{1-e^{-at}} \tag{17}$$

In (17), $\Re^d$ is the desired value of RoCoF. Equation (17) estimates the required power capacity of storage based on the assumption that the ΔP remains constant after the disturbance. This assumption is true to the extent that the power output of conventional generators does not change significantly just after the disturbance due to time delay associated with the droop and turbine-governor. In fact, the power output of steam turbine based generation plants can vary (not very-significantly) after the disturbance as the response time is not very large [25]. Hence, to accurately estimate the required power capacity, a region reduction iterative algorithm (RRIA) is developed. The RRIA uses the size estimated in (17) as an initial guess and iteratively estimates the required capacity as given in (18) and (19).

$$\overline{P_{ir}}(\nu) = (\psi_{min}(\nu) + \psi_{max}(\nu))/2 \tag{18}$$

$$\begin{aligned} \psi_{min}(\nu+1) &= \psi_{min}(\nu)\mathbf{1}_{\{\Re(\nu)<\Re^d\}} + \overline{P_{ir}}(\nu)\mathbf{1}_{\{\Re(\nu)\geq\Re^d\}} \\ \psi_{max}(\nu+1) &= \psi_{max}(\nu)\mathbf{1}_{\{\Re(\nu)>\Re^d\}} + \overline{P_{ir}}(\nu)\mathbf{1}_{\{\Re(\nu)\leq\Re^d\}} \\ \textit{and} \qquad & \varepsilon(\nu) = \psi_{max}(\nu) - \psi_{min}(\nu) \end{aligned} \tag{19}$$

In (18) and (19), ν is the iteration, ψ_{min} and ψ_{max} are the lower and upper boundaries of the solution region, and ε is the gap between the lower and upper boundary. The boundaries are adaptive which are updated during each iteration in the direction to get closer to the solution. The iterative process continues until the boundaries reach at the solution, i.e., $\varepsilon(\nu) \leq \varepsilon_o$. The solution of RRIA is the required power capacity of ESS.

Flowchart of RRIA is shown in Fig. 5. In the first step, the variables are initialized, i.e., $\Re^d = 0.5Hz/s$, $\nu = 1$, $\varepsilon_o = 0.000001pu$, $\psi_{min}(1) = 0$, and $\psi_{max}(1) = \overline{P_{ir}}$ (estimated using (17)). In the second step, $\overline{P_{ir}}(1)$ and $\varepsilon(1)$ are estimated. The error, $\varepsilon(1)$, (which is defined as the gap between the upper and lower boundary of solution) is then compared with the ε_o. If the error is more than the minimum allowable value the algorithm selects the nominal power of IR reserve as $\overline{P_{ir}}(1)$ and simulates the system and estimates RoCoF $\Re(1)$. The RoCoF, $\Re(1)$, is then compared with the desired value of RoCoF, $\Re^d$ and the upper and lower boundaries of the solution get updated accordingly. The iterative process continues until the upper and lower boundaries of the solution overlap, i.e., $\varepsilon(\nu) \leq \varepsilon_o$.

It is worth mentioning that magnitude of RoCoF is considered in this work for the analysis. It has no effect on the obtained results but adds simplicity in analysis.

An ESS is entirely characterized by power capability (MW rating) and energy capacity (MWh rating). The energy capacity of ESS can be calculated using (20).

$$\overline{E_{ir}} = \frac{\gamma \int_{t0_{ir}}^{tf_{ir}} P_{ir}(t)dt \times \eta_{ir}^c}{3600} + \frac{\gamma \int_{t0_{ir}}^{tf_{ir}} P_{ir}(t)dt}{3600 \times \eta_{ir}^d} \tag{20}$$

In (20), $t0_{ir}$ and tf_{ir} are the start and end of inertial response stage. Since the unit of time is second, a factor 3600 is used to convert it to MWh, and γ is used to account for SoC limits.

3.2 Sizing ESS for PFR

The purpose of the primary frequency reserve is to automatically arrest frequency after an event and bring it back within the permissible limits. The primary frequency reserve must be deployed linearly within 30 s for frequency deviation of $\pm 200mHz$ as deployed in the Continental Europe [11]. Moreover, the reserve must be capable of delivering the service for 15 min.

The steady-state frequency after an event can be estimated using (21).

$$\Delta f_{ss} = \frac{-\Delta P + \overline{P_{pfr}}(1-e^{-at})}{\sum_{i=1}^{n} 1/R_i} \tag{21}$$

In (21), Δf_{ss} is the steady state frequency error, and R is the droop. The required rated power capacity of ESS to lift the steady state frequency to Δf_{ss}^d can be estimated by (22).

$$\overline{P_{pfr}} = \lceil \Delta f_{ss}^d \times \sum_{i=1}^{n} 1/R_i - \Delta P \rceil \tag{22}$$

Since the response time of ESS is very small (typically less than 1s), the factor $1-e^{-at}$ can be ignored in primary frequency reserve calculations. The energy capacity of primary frequency reserve can be calculated using (23).

$$\overline{E_{pfr}} = \frac{\gamma \int_{t0_{pfr}}^{tf_{pfr}} P_{pfr}(t)dt \times \eta_{pfr}^c}{3600} + \frac{\gamma \int_{t0_{pfr}}^{tf_{pfr}} P_{pfr}(t)dt}{3600 \times \eta_{pfr}^d} \tag{23}$$

In (23), $t0_{pfr}$ and tf_{pfr} are the start and end time of PFR.

Since there are various fast responsive technologies which are suitable for IR and PFR. So, it is vital to make an economical comparison to find out the most suitable storage technology. Two major costs are associated with the ESS, i.e., cost related to energy capacity and the cost related to power capacity. The initial investment cost of ESS is estimated using (24).

$$C_{ir/pfr}^{inv} = C_{ir/pfr}^{p} \overline{P_{ir/pfr}} + \overline{E_{ir/pfr}} C_{ir/pfr}^{e} \tag{24}$$

In (24), C^{inv} is the initial investment cost in \$, C^p is the cost associated with power capacity in \$/MW, and C^e is the cost associated with power capacity in \$/MWh. The C^p is account for the cost of power conversion system (i.e., converter) and other equipment required to integrate and operate ESS in the AC grid. Since various storage technologies have different life cycles, for example, SCES has higher life cycles compared to BES. Therefore, the initial investment cost might not give an accurate comparison. Therefore, the cost per cycle is used for comparison. The cost per cycle can be calculated using (25).

$$C_{ir/pfr}^{inv/cyc} = C_{ir/pfr}^{inv} / N_{ir/pfr}^{cyc} \tag{25}$$

In (25), $C_{ir/pfr}^{inv/cyc}$ is the cost per cycle and $N_{ir/pfr}^{cyc}$ is the life cycles.

3.3 Sizing ESS for IR-PFR

Sizing of ESS for both IR and PFR is based on the results the previously mentioned techniques, i.e., sizing ESS for IR and sizing ESS for PFR.

$$\overline{P_{ir}^{ir+pfr}} = \left(\overline{P_{ir}} - \overline{P_{pfr}}\right)\mathbf{1}_{\{\overline{P_{ir}}\geq\overline{P_{pfr}}\}} + \overline{P_{ir}}\mathbf{1}_{\{\overline{P_{ir}}<\overline{P_{pfr}}\}} \tag{26}$$

$$\overline{P_{pfr}^{ir+pfr}} = \overline{P_{pfr}} \tag{27}$$

$$\overline{E_{ir}^{ir+pfr}} = \frac{\gamma \int_{t0_{ir}}^{tf_{ir}} P_{ir}^{ir+pfr}(t)dt \times \eta_{ir}^c}{3600} + \frac{\gamma \int_{t0_{ir}}^{tf_{ir}} P_{ir}^{ir+pfr}(t)dt}{3600 \times \eta_{ir}^d} \tag{28}$$

$$\begin{aligned} \overline{E_{pfr}^{ir+pfr}} = &\left(\frac{\gamma \int_{t0_{ir}}^{tf_{ir}} P_{pfr}^{ir+pfr}(t)dt \times \eta_{pfr}^c}{3600} + \frac{\gamma \int_{t0_{ir}}^{tf_{ir}} P_{pfr}^{ir+pfr}(t)dt}{3600 \times \eta_{pfr}^d} + \right. \\ &\left. \frac{\gamma \int_{t0_{pfr}}^{tf_{pfr}} P_{pfr}^{ir+pfr}(t)dt \times \eta_{pfr}^c}{3600} + \frac{\gamma \int_{t0_{pfr}}^{tf_{pfr}} P_{pfr}^{ir+pfr}(t)dt}{3600 \times \eta_{pfr}^d} \right) \mathbf{1}_{\{\overline{P_{ir}}\geq\overline{P_{pfr}}\}} + \\ &\left(\frac{\gamma \int_{t0_{ir}}^{tf_{ir}} \left(P_{pfr}^{ir+pfr} - P_{ir}^{ir+pfr}\right)(t)dt \times \eta_{pfr}^c}{3600} + \frac{\gamma \int_{t0_{pfr}}^{tf_{pfr}} P_{pfr}^{ir+pfr}(t)dt \times \eta_{pfr}^c}{3600} \right. \\ &\left. \frac{\gamma \int_{t0_{ir}}^{tf_{ir}} \left(P_{pfr}^{ir+pfr} - P_{ir}^{ir+pfr}\right)(t)dt}{3600 \times \eta_{pfr}^d} + \frac{\gamma \int_{t0_{pfr}}^{tf_{pfr}} P_{pfr}^{ir+pfr}(t)dt}{3600 \times \eta_{pfr}^d} \right) \mathbf{1}_{\{\overline{P_{ir}}<\overline{P_{pfr}}\}} \end{aligned} \tag{29}$$

In (26)-(27), $\overline{P_{ir}^{ir+pfr}}$, $\overline{P_{pfr}^{ir+pfr}}$, $\overline{E_{ir}^{ir+pfr}}$, and $\overline{E_{pfr}^{ir+pfr}}$ are the power and energy capacities of ESS when designed for both IR and PFR

Table 1 Parameters of CPS, *HPS*

Power generation unit	Power rating (MVA)	Active power (MW)	Inertia constant (s)	Number of units (–)
G1	750, *750*	600, *600*	10.0128, *10.0128*	3/2*, *3/2**
G2	640, *0*	400, *0*	8.3213, *0*	4, *0*
G3	384, *0*	250, *0*	6.9344, *0*	2, *0*
G4	474, *158*	300, *100*	6.6722, *6.6722*	3, *1*
RES	0, *1340*	0, *850*	0, *0*	–, –
Total	2248, *2248*	1550, *1550*	8.3010, *3.8095**	–, –
Total*	1998, *1998*	–, –	8.0868*, *3.033**	–, –

* The equivalent values after the loss of one unit of G1

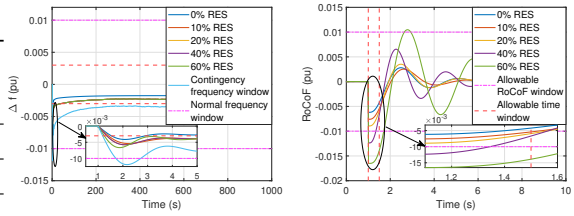

(a) (b)

Fig. 6: System dynamic responses (a) Frequency (b) RoCoF.

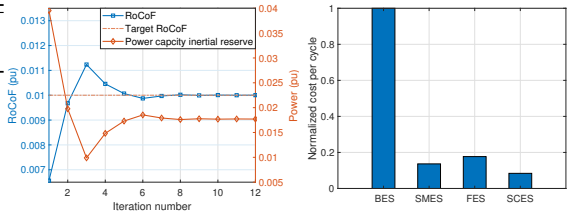

(a) (b)

Fig. 7: (a) RRIA (b) Cost per-cycle.

services. Equation (26) suggests that if the required nominal power capacity of IR reserve is more than PFR reserve then the power capacity of IR reserve in IR+PFR services is $\overline{P_{ir}} - \overline{P_{pfr}}$. Thus, in this case, sum of $\overline{P_{ir}}$ and $\overline{P_{pfr}}$ is the total required power capacity of the IR reserve. Both IR and PFR reserves provide inertial response and after providing the inertial response service the output of IR reserve becomes zero while PFR reserve continues to provide the PFR service.

4 Results and Discussions

A generic 12-bus system is used to study the effectiveness of the proposed methodology. The system without the RES is termed as conventional power system (CPS) and generator data is given in Table 1. The penetration of RES is increased from 0 to 60%. The system with 60% penetration level of RES is denoted here as a hybrid power system (HPS). The parameters of HPS are also given in Table 1. It can be seen from Table 1 that the system equivalent inertia decreased with the replacement of conventional generation plants with RES.

The power system should be planned to remain stable under contingencies like the loss of major components. The largest generator is G1 (there are three units of G1 in total). The loss of one unit of G1 is considered as the major disturbance in the system. The major disturbance is created in the simulation in such a way that it causes a power deficit of 200 MW and reduces the system inertia. The variation in system frequency and RoCoF in response to major disturbance are shown in Fig. 6. The frequency and RoCoF are constrained within the adequate limits for and up to 20% penetration level of RES. The RoCoF falls outside the acceptable limit for both 40% and 60% penetration of RES. In case of 40% penetration of RES, the RoCoF becomes smaller than 0.01 pu before the activation of RoCoF relay. Thus, the system fulfills the stable operation criteria upto 40% penetration of RES. For 60% penetration of the RES, the RoCoF remains higher than 0.01 pu for more than 500 ms. This may result in generation disconnection and subsequently lead to system blackout. In this study, no RoCoF relay is implemented that is why the system is running even with the RoCoF of 0.01 pu for higher than 500 ms. It is evident from Fig. 6 that the RoCoF and steady state deviation in frequency increase with the larger amounts of RES. This is due to fact that the replacement of conventional generation by RES reduces the system inertia, thus making system weak and vulnerable to higher RoCoF, leading to larger frequency deviations. The steady-state frequency and RoCoF of the system with 60% RES fall outside the nominal operating windows. Therefore, ESS should be deployed to limit the RoCoF and bring the steady-state frequency error within the allowable range. In this study, the ESS is designed for the system with 60% penetration of RES.

4.1 ESS for Inertial Response

The methodology developed in Section 3.1 is used here to determine the appropriate size of ESS to limit the RoCoF to the desired limits. In the first step, the size is estimated analytically. This estimated size is used as an initial guess for RRIA. The variation in RoCoF and power capacity in each iteration is given in Fig. 7a. It can be observed that the RRIA converged at RoCoF of 0.01 pu.

In order to determine the most suitable storage technology for providing IR, an economical comparison is carried out based on the cost per-cycle. It is important to note that initial investment cost and number of life cycles of different storage technologies are significantly different [7]. Thus a comparison only based on the initial investment cost might be misleading. Therefore the cost per cycle is used instead to compare various storage technologies. The cost per-cycle of each storage technology (BES, SCES, SMES, and FES) is calculated based on the power cost, energy cost, and number of life cycles as discussed in Section 3. The results are given in Fig. 7b. It is evident from Fig. 7b that the SCES is the most economical compared to other rapid responsive storage technologies. The BES is the most expensive due to the lower number of cycles with high cost related to power capacity. The required power and energy capacities of SCES to fulfill the dynamic planning requirement are 35.4 MW and 0.1363 MWh, respectively.

To demonstrate the effectiveness of the proposed methodology, the SCES with estimated power and energy capacities is deployed in the HPS to provide IR support. The major disturbance is applied and the variations in RoCoF and frequency with and without SCES are recorded and depicted in Fig. 8a and Fig. 8b, respectively. It can be seen clearly that the SCES effectively limits the RoCoF to 0.01 pu (before the triggering of the RoCoF relay). It is important to note that initially the RoCoF is higher with SCES (like the system without SCES). This is because during this time, the SCES is not active due to the time delay associated with the measurement and activation system. The SCES also arrests the frequency before it falls outside the contingency frequency range. It is also noticeable that the fall in frequency is also slowed down by SCES(because of limiting the RoCoF). It is evident from the above results that the methodology developed in Section 3.1 can accurately estimate rated power capacity of SCES.

The variation in power output and SoC of SCES are given in Fig. 8c. The graph's left y-axis represents the variation in power output of SCES with time and the rated power capacity of SCES. The graph's right y-axis represents the variation in SoC of SCES with time (on x-axis) and the allowable SoC limits. The SCES ramps up to full capacity after receiving the signal from the measurement

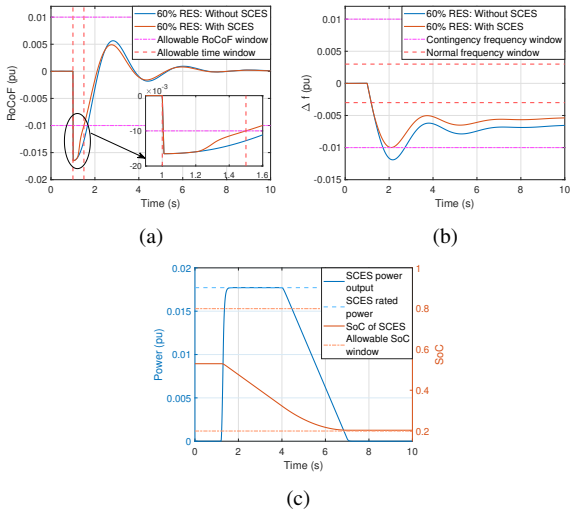

Fig. 8: System dynamic responses for IR (a) RoCoF (b) Frequency (c) Power and SoC.

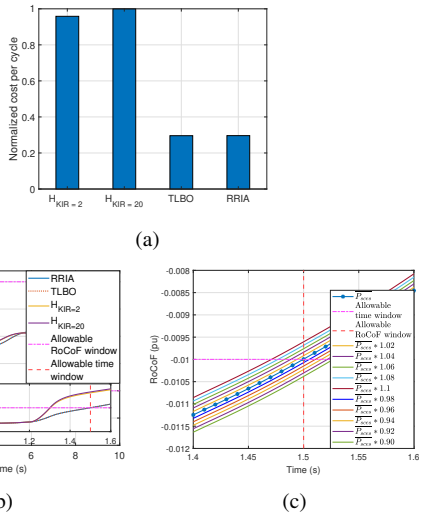

Fig. 9: Comparative results for IR (a) Cost per-cycle (b) RoCoF (c) RoCoF for various SCES sizes.

and identification system. The SCES power output remains into the full capacity up to 3 s from the occurrence of event. Afterwards the power output of SCES is ramped down and reaches to zero after 6 s of the occurrence of fault. The SCES is disabled linearly to avoid another frequency dip. It is evident from the figure that the SCES is operated within the rated power capacity as the power output of SCES is within the rated power capacity. Fig. 8c also depicts that the SoC of SCES reaches to minimum allowable value at the end of service. It is worth noting that a value of SoC higher than the minimum allowable value at the end of service means over-sizing. Similarly, a value of SoC lower than the minimum allowable value at the end of service represents under-sizing. It is evident from the variation in SoC in Fig. 8c that the proposed methodology accurately estimates the energy capacity of SCES.

The time for the operation of SCES (i.e., 6 s) is selected based on the Australian electricity market operator (AEMO) fast frequency service. A different dispatch and detachment scheme can also be used as per the transmission system operator requirements. The different dispatch and detachment scheme will not affect the effectiveness of the proposed methodology, rather it would result in different energy capacity of SCES.

To assess the accuracy of the proposed sizing methodology, sizing of SCES is done using the methodology given in [12](named as base case in the following discussion) and teacher learner based optimization (TLBO) algorithm. The cost function used by TLBO to determine the size of SCES to limit the RoCoF is given in Appendix A. The variation in the cost function of TLBO is given in Fig. 14a (given in Appendix A).

The normalized cost per cycle of SCES estimated using the base case methodology, TLBO, and the proposed methodology is shown in Fig. 9a. The expressions; $S_{ESS_{HKIR=2}}$ and $S_{ESS_{HKIR=20}}$ correspond to the base case methodology are given in Appendix B. The per-cycle cost associated with base case methodology is quite large compared to the proposed methodology and the TLBO. It is evident that the per-cycle cost of SCES estimated using the TLBO is equal to the proposed methodology. The SCES with the sizes estimated by the base case, proposed methodology and TLBO was deployed in the system and major disturbance was created for each case. The variation in RoCoF with the size estimated using the proposed methodology in comparison to the sizes estimated using base case methodology and TLBO is shown in Fig. 9b. It is evident from Fig. 9b that the proposed methodology and TLBO effectively limit the RoCoF to 0.01 pu as per the designed criteria. While the base case methodology limits the RoCoF to smaller values which is due to a larger size of storage, which will incur more cost (as evident from Fig. 9a). Therefore, it should be worth noting that the proposed methodology can accurately estimate the appropriate size of storage without using any metaheuristic optimization algorithm (which requires more computational effort).

To further access the accuracy of the proposed sizing methodology, a local comparison is also made in which the system is operated for different sizes of SCES. The estimated SCES size is increased and decreased in small steps. The variation in system RoCoF to major disturbance is shown in Fig 9c. It can be observed from the given results that the proposed method estimates the size of SCES accurately as it limits the RoCoF to 0.01 pu. The SCES with rating smaller than the estimated size fails to limit the RoCoF before the activation time of the relay (under-sizing). While the SCES rating greater than the estimated size (over-sizing), limits the RoCoF to values smaller than 0.01 pu. It is understood that over-sized SCES is associated with higher cost, though the RoCoF is limited well within the threshold value.

4.2 *ESS for Primary Frequency Regulation*

The power and energy capacities of four storage technologies have been calculated using the methodology developed in Section 3.2 to provide the PFR. The normalized cost per cycle is also estimated and given in Fig. 10a. It can be observed that the cost is minimum for BES. Hence, BES is economically more feasible for providing PFR. The power and energy capacities of BES are 28.74 MW and 23.7959 MWh, respectively. The BES has the lowest cost associated with the energy capacity, and the required energy capacity for PFR is also high, making it the most economical option among four technologies for PFR service. The cost is highest for FES as both energy cost and power costs are higher for FES. Hence, compared to the storage technologies with a higher power density (SCES, FES, and SMES), the energy-dense storage (e.g., BES) is more economical for the services for the required power and energy capacities are comparable.

To validate the proposed method, the BES with the rated power and energy capacities is deployed in the HPS. The major disturbance is created in the system and the variations in system frequency are recorded and given in Fig. 10b. It can be observed that the BES successfully lifts the frequency to the nominal frequency limit. The variations in the SoC and power output of BES with respect to time are shown in Fig. 10c. The graph's left y-axis shows the variation in power output of BES. The variation in SoC is depicted on the graph's right y-axis. BES is assumed to be initially charged at 53%

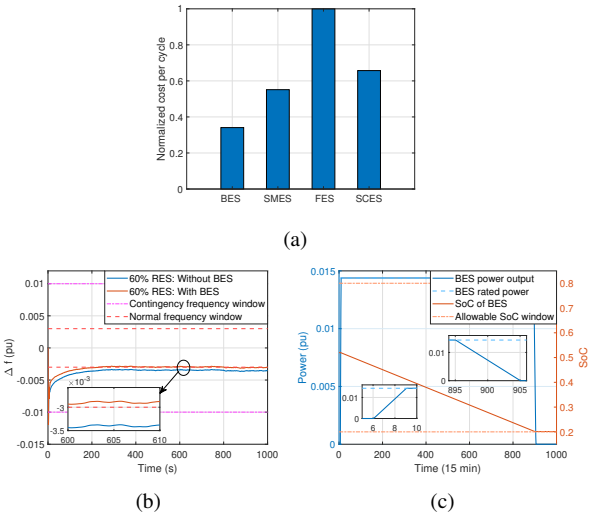

(a) (b) (c)

Fig. 10: PFR results (a) Cost per-cycle (b) Frequency (c) Power and SoC.

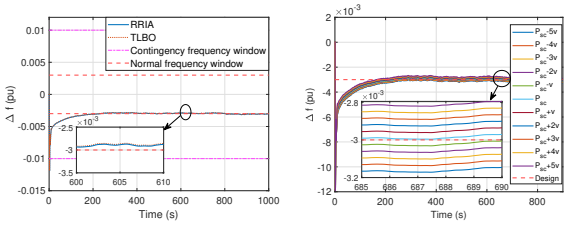

(a) (b)

Fig. 11: Comparative results for PFR (a) Frequency (b) Variation in frequency for various BES sizes.

Table 2 ESS types and capacities for IR, PFR and IR+PFR services

Service	Storage Type	Power Capacity (MW)	Energy Capacity (MWh)
IR	SCES	35.4	0.1363
PFR	BES	28.74	23.8
IR+PFR	BES-SCES	28.74, 6.66	23.71, 0.0256

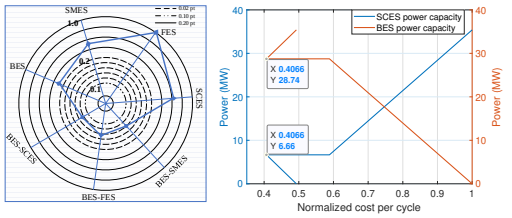

(a) (b)

Fig. 12: Economic analysis for IR+PFR (a) Cost per-cycle (b) Variation in cost with the size of BES and SCES in HESS.

as it is responsible for both upward and downward regulation services. The SoC of BES settles at 20% at the end of the operation as the BES is designed to operate between 20% and 80% SoC. It is evident from end of service SoC that the energy capacity of BES is accurately sized. The reason is that a smaller or larger capacity would have resulted in end of service SoC to be lower or greater than the minimum SoC value. The BES starts the operation after 5 s of the disturbance as typically PFR stage and IR stage are distinct. However, they can be partially or fully overlapped depending on the requirements for the system operator. The power output of the BES is similar to the operation of real BES frequency responses given in [21]. It can be observed from Fig. 10c that the BES is fully deployed in the system at 9 s. The response time of BES is much faster and it can be dispatched fully less than 0.5 s (considering BES time delay, the delay introduced by the power converters, and measurement and identification system). To prevent the BES from deterioration due to fast discharging, slow dispatch of BES has been considered. Even dispatching of BES at a faster rate would not affect the validity of the proposed methodology. Instead, that would increase the required energy capacity of BES. The battery is detached linearly from the system after the PFR operation. The instantaneous disconnection may create large power deficit which could cause contingency condition in the system.

To assess the accuracy of the proposed sizing methodology of ESS for PFR, sizing of BES is also done using TLBO. The variation in the cost function is given in Fig. 14b (given in Appendix A). The variation in frequency with the size estimated of BES using the proposed methodology in comparison to the size estimated using TLBO is shown in Fig. 11a. It is evident that the BES size estimated using the proposed methodology and the TLBO effectively lifts the frequency to the desired level. An over-sized storage would have resulted in steady state deviation in frequency to be more than the desired value, while an under-sized BES would have failed to lift the steady state frequency to the desired value. Thus, the proposed methodology accurately estimates the size of BES to provide PFR without using metaheuristic technique (which are difficult to program and requires more computational effort).

The accuracy of the proposed methodology to size ESS for PFR is also assessed by making a local comparative analysis. The estimated size of BES is increased and decreased in small steps to get the sample sizes. The variation in system frequency for different sizes of BES is shown in Fig. 11b. It can be observed that the BES ratings smaller than the estimated size fail to lift the frequency to designed limit (i.e. under-sizing). While the BES ratings larger than the estimated size lift the frequency higher than the designed limit (this may be beneficial for the system but at higher expenses).

4.3 ESS for Inertial and Primary Frequency Regulation

The sizes of four ESS technologies are estimated for both IR and PFR services. The cost per cycle for the four rapid responsive storage technologies (BES, SCES, FES, and SMES) and possible hybrid energy storage systems (BES-SCES, BES-SMES, BES-FES) are given in Fig. 12a. It can be observed that the hybrid storage combinations are more economical compared to single storage systems. It is evident from Fig. 12a that the BES-SCES is the most economically feasible for IR-PFR among all storage technologies. This is due to the fact that the BES and SCES have complementary power and energy characteristics. Unlike IR (which requires high power and small energy capacity) and PFR (which requires high energy capacity), IR-PFR requires both high energy and high power thus making HESS most economical. The variation in cost corresponding to different power capacities of BES and SCES is given in Fig. 12b. It is important to note that the cost is calculated based on the power capacity, energy capacity, and number of cycles. It is evident that the minimum cost corresponds to the BES: 28.74 MW, and SCES: 6.66 MW. The power and energy capacities of BES and SCES required for IR, PFR and IR-PFR services are given in Table 2.

The variation in the system frequency with respect to the major disturbance is shown in Fig. 13a. The HESS effectively maintains the frequency within the contingency frequency window. Moreover, the HESS maintains the steady-state frequency within the standard

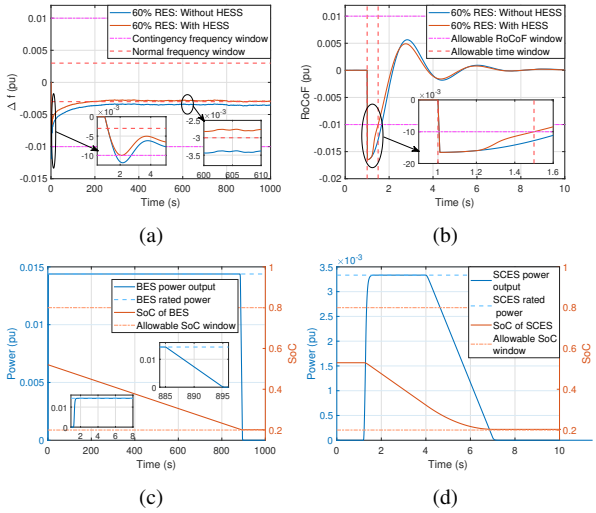

Fig. 13: System dynamic responses for IR+PFR (a) Frequency (b) RoCoF (c) Power and SoC of BES (d) Power and SoC of SCES.

frequency window. The variation in RoCoF is shown in Fig. 13b. The HESS lifts the RoCoF within 0.1 pu before the activation of RoCoF relay. This shows the accuracy of the power capacities of the BES and SCES deployed in HESS storage.

The variation in power output and SoC of BES and SCES (deployed to form HESS) are shown in Fig. 13c and Fig. 13d, respectively. In Fig. 13c and Fig. 13d, the graph's left y-axis represents the variation in power output of BES and SCES, while the graph's right y-axis represents the variation in SoC. It can be seen that the BES and SCES start supplying the power after a small delay (due to event measuring and identification system). The SCES is disconnected from the system (after 6 s of the fault), and its output is decreased linearly to avoid the sudden power deficit. The BES supplied power for 900 s and removed linearly to avoid the sudden power deficit. It is evident that HESS operated within the rated power capacity as both BES and SCES are operated within the rated power capacities. It can also be seen that the SoC of both SCES and BES remain within the allowable SoC limits. In this study, the BES and SCES are considered to operate between 20% and 80% of SoC. It is important to note that SCES and BES can be operated within any defined SoC limits, and this will not affect the accuracy of the proposed methodology. The SoC of both BES and SCES reach to minimum value of SOC at the end of service which shows the accuracy to estimated energy capacity of HESS.

It is evident from the above results and discussions that the proposed methodology can accurately estimate the power and energy capacities of ESS for IR, PFR, and IR-PFR services. Moreover, the proposed operation strategy effectively operates the HESS while fulling the constraints inflicted by the power and energy ratings. It is also clear that the SCES and BES are economical for IR and PFR, respectively. The HESS (BES-SCES) is more economical for IR-PFR.

5 Conclusion

In this paper, a methodology is developed to determine the sizes of energy storage system (ESS) for inertial response (IR) and primary frequency regulation (PFR) in small power system with high penetration of renewable energy sources. The proposed methodology estimated the required power and energy capacities of ESS and determined the most economical storage technologies for IR, PFR, and IR-PFR services. The proposed method is applied to determine the sizes of commonly used rapid responsive energy storage technologies such as battery energy storage (BES), flywheel energy storage (FES), supercapacitor energy storage (SCES), and superconducting magnetic energy storage (SMES). The possible hybrid energy storage systems (HESS) such as BES-SCES, BES-SMES, and BES-FES are also considered in this work. The highlights of this research can be summarized as follows:

- A novel methodology has been developed to size the energy storage to provide inertial response and primary frequency regulation. A region reduction iterative algorithm (RRIA) is developed to size the storage for IR. The sizing of ESS for PFR is done analytically using the power system frequency characteristics.
- From the numerical results it is found that SCES and BES are most economical for IR and PFR, respectively. Besides, BES-SCES hybrid system is the most economical for IR-PFR. It has been shown that ESS with estimated sizes can effectively limit the RoCoF and steady state frequency deviation as per designed criteria while fulfilling the operational constraints.
- The accuracy of the proposed methodology is assessed by making comparative study of the proposed methodology with the teacher learner based optimization (TLBO) algorithm and sizing methodology given in literature.
- It has been shown that the proposed methodology accurately estimates the sizes of ESS without utilizing any metaheuristic algorithm which requires specialized expertise to implement and high computational effort.
- The proposed methodology is neither specific to the studied test system nor to any storage technology, but it can be extended to any power system including any type of storage technology.

Appendix A

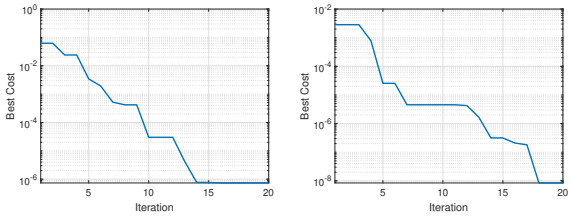

Fig. 14: Variation in cost function solved using TLBO for (a) IR (b) PFR .

The objective function J for the TLBO is formulated as follows.

$$obj: J = \sqrt{(J_1(\boldsymbol{X}) - J_2)^2} \rightarrow \min \tag{30}$$

$$s.t. \begin{cases} \boldsymbol{g}_\ell(\boldsymbol{X}) = 0 & \ell = 1,2,,...,m \\ \boldsymbol{h}_\iota(\boldsymbol{X}) \leq 0 & \iota = 1,2,,...,q \end{cases} \tag{31}$$

where

$$\boldsymbol{X} = \left[\overline{P_{ir}}\ \overline{P_{pfr}}\ \overline{E_{ir}}\ \overline{E_{pfr}}\right] \tag{32}$$

The first term in the objective function J_1 represents the RoCoF and frequency of the system and J_2 represents the desired value of RoCoF and/or frequency. The equality constraints are represented by $\boldsymbol{g}$ and in-equality constraints are represented by $\boldsymbol{h}$. The equality and in-equality constraints are inflicted by the storage, conventional generation system and RES.

Appendix B

$$S_{ESS} = \frac{H_{target} - H_{PS1}}{H_{ESS_{KIR=(1,2,20)}} - H_{target}} \tag{33}$$

$$H_{target} = \frac{\Delta P_b}{S_{sys1}} \times \frac{f_o}{2} \times \left(\frac{df}{dt}\right)^{-1} \quad (34)$$

$$H_{ESS_{KIR=20}} = 1.736 \times 10^4 \times \Delta P_b^{-1.156} \quad (35)$$

$$H_{ESS_{KIR=1}} = 19.81 \ \ and \ \ H_{ESS_{KIR=2}} = 39.41 \quad (36)$$

The definition of each variable used above can be found in [12]. The values of the unknown parameters are calculated using following data to estimate the size of energy storage.

$\Delta P_b = 200\ MW$, $S_{sys1} = 1998\ MVA$, $f_o = 50\ Hz$, $\frac{df}{dt} = 0.5\ Hz/s$, $H_{PS1} = 3.03\ s$, and $H_{target} = 5.005\ s$.

6 References

[1] Akram U., Nadarajah M., Raza M Q., Shah R., Milano F.: 'RoCoF restrictive planning framework and wind speed forecast informed operation strategy of energy storage system', *IEEE Transactions on Power Systems*, 2020.

[2] AEMO. : 'Update report: Black system event in South Australia on 28 September 2016', *Adelaide, South Australia*, 2016.

[3] Statnett, Svenska Kraftän, Fingrid, Energinet.dk: 'Challenges and opportunities for the Nordic power system', *Technical Report*, 2016.

[4] Milano F., Dörfler F., Hug G. Hill, D. J., and Verbiˆc, G. : 'Foundations and challenges of low-inertia systems', in *IEEE Power Systems Computation Conference (PSCC)*, 2018, pp. 1-25.

[5] RG-CE System Protection & Dynamics Subgroup : 'Frequency stability evaluation criteria for the synchronous zone of continental Europe', *Technical Report*, 2013.

[6] ERCOT Concept Paper : 'Future ancillary services in ERCOT', *Technical Report*, 2013.

[7] Akram U., Nadarajah M., Shah R., Milano F.: 'A review on rapid responsive energy storage technologies for frequency regulation in modern power systems', *Renewable and Sustainable Energy Reviews*, 2020, 120, pp. 109626.

[8] Lukic S. M., Wirasingha S. G., Rodriguez F., Cao J., Emadi A.: 'Power management of an ultracapacitor/battery hybrid energy storage system in an HEV', *IEEE Vehicle Power and Propulsion Conference*, 2006, pp. 1-6.

[9] Cao J., Emadi A.: 'A new battery/ultracapacitor hybrid energy storage system for electric, hybrid, and plug–in hybrid electric vehicles', *IEEE Transactions on Power Electronics*, 2012, 27, (1), pp. 122–132.

[10] Cao J., Du W., Wang H., McCulloch M.: 'Optimal sizing and control strategies for hybrid storage system as limited by grid frequency deviations', *IEEE Transactions on Power Systems*, 2018, 33, (5), pp. 5486-5495.

[11] Peng B., Zhang F. Liang J., Ding L., Wu Q.: 'An optimal control and sizing strategy for a coordinated WTG-ES system to provide frequency support', *International Journal of Electrical Power & Energy Systems*, 2019, 133, pp. 251-263.

[12] Knap V., Chaudhary S. K., Stroe D. I., Swierczynski M., Craciun B. I., Teodorescu R.: 'Sizing of an energy storage system for grid inertial response and primary frequency reserve', *IEEE Transactions on Power Systems*, 2016, 31, (5), pp. 3447–3456.

[13] Ramirez M., Castellanos R., Calderon G., Malik O.: 'Placement and sizing of battery energy storage for primary frequency control in an isolated section of the Mexican power system', *Electric Power Systems Research*, 2018, 160, pp. 142-150.

[14] Yao J., Yu M., Gao W., Zeng X.: 'Frequency regulation control strategy for PMSG wind-power generation system with flywheel energy storage unit', *IET Renewable Power Generation*, 2017, 11, (8), pp. 1082-1093.

[15] Magdy G., Mohamed E. A., Shabib G., Elbaset A. A., Mitani Y.: 'SMES based a new PID controller for frequency stability of a real hybrid power system considering high wind power penetration', *IET Renewable Power Generation*, 2018, 12, (11), pp. 1304-1313.

[16] El-Hameed M. A., Elkholy M. M., El-Fergany A. A.: 'Efficient frequency regulation in highly penetrated power systems by renewable energy sources using stochastic fractal optimiser', *IET Renewable Power Generation*, 2019, 13, (12), pp. 1304-1313.

[17] Akram U., Khalid M.: 'A coordinated frequency regulation framework based on hybrid battery-ultracapacitor energy storage technologies', *IEEE Access*, 2017, 6, pp. 7310-7320.

[18] Akram U., Shah R., Nadarajah M.: 'Hybrid energy stoarage system for frequency regulation in microgrids with source and load uncertainties', *IET Generation, Transmission & Distribution*, 2019, 13(20), pp. 5048-5057.

[19] Dreidy, M., Mokhlis, H. Mekhilef, S.: 'Inertia response and frequency control techniques for renewable energy sources: A review', *Renewable and Sustainable Energy Reviews*, 2017, 69, pp. 144-155.

[20] Meng L., Zafar J., Khadem S. K., Collinson A., Murchie K. C. Coffele, F., Burt G. : 'Fast frequency response from energy storage systems-a review of grid standards, projects and technical issues', *IEEE Transactions on Smart Grid*, 2020, 11, (2), pp. 1566-1581.

[21] Brogan P. V., Best R. J., Morrow D. J., McKinley K., Kubik M. L.: 'Effect of BESS response on frequency and RoCoF during under frequency transients', *IEEE Transactions on Power Systems*, 2019, 34, (1), pp. 575-583.

[22] Fathi A., Shafiee Q., Bevrani H.: 'Robust frequency control of microgrids using an extended virtual synchronous generator', *IEEE Transactions on Power Systems*, 2018, 33, (6), pp. 6289-6297.

[23] Kundur P., Balu N. J., Lauby M. G.: 'Power System Stability and Control', *New York, NY: USA, McGraw-Hill*, 1994.

[24] Adamczyk A., Altin M., Göksu Ö., Teodorescu R., Iov F. : 'Generic 12-bus test system for wind power integration studies', in *IEEE European Conference on Power Electronics and Applications*, 2013, pp. 1-6.

[25] Bhuiyan M., Dinakar S.: 'Comparing and evaluating frequency response characteristics of conventional power plant with wind power plant.', in *Chalmers University of Technology*, 2008.